



# A non-singular integral equation formulation to analyse multiscale behaviour in semi-infinite hydraulic fractures

E. V. Dontsov<sup>1,‡</sup> and A. P. Peirce<sup>1,†</sup>

<sup>1</sup>Department of Mathematics, University of British Columbia, Vancouver, BC V6T 1Z2, Canada

(Received 2 June 2015; revised 20 July 2015; accepted 29 July 2015)

This study revisits the problem of a steadily propagating semi-infinite hydraulic fracture in which the processes of toughness-related energy release, viscous dissipation and leak-off compete on multiple length scales. This problem typically requires the solution of a system of integro-differential equations with a singular kernel, which is complicated by the need to capture extremely disparate length scales. In this study the governing equations are rewritten in the form of one non-singular integral equation. This reformulation enables the use of standard numerical techniques to capture the complete multiscale behaviour accurately and efficiently. This formulation also makes it possible to approximate the problem by a separable ordinary differential equation, whose closed-form solution captures the multiscale behaviour sufficiently accurately to be used in practical applications. We also consider a similar reformulation of the equations governing the propagation of a buoyancy-driven semi-infinite hydraulic fracture. The resulting numerical solution is able to capture the near-tip multiscale behaviour efficiently and agrees well with published solutions calculated in the large-toughness limit.

**Key words:** boundary layer structure, magma and lava flow, porous media

## 1. Introduction

A detailed near-tip analysis of a planar hydraulic fracture shows (Peirce & Detournay 2008) that the governing equations reduce to those of a steadily propagating semi-infinite hydraulic fracture under conditions of elastic plane strain. It is therefore important to analyse the problem of a semi-infinite hydraulic fracture, as it governs the behaviour of the tip region of arbitrarily shaped finite hydraulic fractures and influences their global behaviour. Recognizing the necessity of accurate

† Email address for correspondence: [peirce@math.ubc.ca](mailto:peirce@math.ubc.ca)

‡ Department of Civil and Environmental Engineering, University of Houston, Houston, TX 77204, USA.

fracture tip modelling, the hydraulic fracturing methodology known as the implicit level set algorithm (ILSA) (Peirce & Detournay 2008) was developed to embed the solution of the appropriate semi-infinite hydraulic fracture into every fracture tip element. This procedure is shown to produce accurate results even on a relatively coarse mesh (Lecampion *et al.* 2013). This technique has also been used in the context of the extended finite element method to model the propagation of hydraulic fractures (Gordeliy & Peirce 2013). It is therefore important to develop a fast and accurate solution methodology to solve the semi-infinite fracture problem so that it can be used to increase the performance of various hydraulic fracturing simulators in this multiscale environment.

To analyse the problem of a propagating semi-infinite hydraulic fracture, we adopt a mathematical model that assumes that (i) the fracturing fluid is Newtonian, (ii) the fluid front coincides with the fracture tip (i.e. there is no fluid lag), (iii) the material is brittle and is linear elastic, and (iv) the leak-off is modelled by a one-dimensional diffusion process via Carter's model, which is applicable when the diffusion length scale is much smaller than the fracture length (Carter 1957). Other studies that involve a steadily propagating semi-infinite hydraulic fracture consider the effects of power-law fluid (Desroches *et al.* 1994; Lenoach 1995), account for the fluid lag (Garagash & Detournay 2000) or include poroelastic effects (Kovalyshen & Detournay 2013). However, most of these studies focus on some limiting regimes of propagation (Detournay 2004). The first problem we consider has already been addressed in Garagash, Detournay & Adachi (2011), where a special numerical scheme with built-in asymptotic solutions was used. Unfortunately, due to the complexity of that numerical approach, it is not possible to obtain a rapid solution for the purpose of embedding it into a hydraulic fracturing simulator that exploits the tip asymptotics such as the ILSA strategy (Peirce & Detournay 2008). A partial solution was obtained (Peirce 2015) in which the pre-computed semi-infinite fracture toughness-to-viscous solution was interpolated to capture the multiscale fracture tip behaviour in the hydraulic fracturing simulator ILSA. In this case the tip solution without leak-off was utilized, so that one-dimensional interpolation could be used to provide satisfactory precision, albeit at a noticeably increased computational cost. A similar interpolation-based scheme for the tip solution with leak-off does not seem feasible since two-dimensional interpolation is required. This would substantially complicate the algorithm, might introduce significant numerical errors and would dramatically degrade the overall computational performance of the hydraulic fracture simulator.

To address this problem, following Garagash *et al.* (2011), this study first outlines the equations that govern the problem of a semi-infinite hydraulic fracture with leak-off in § 2.1. Then, § 2.2 reformulates the original governing integro-differential equations with a singular kernel used in Garagash *et al.* (2011) in the form of a single integral equation with a non-singular kernel. This allows us to use standard numerical techniques to obtain the multiscale solution rapidly. In § 2.3 we use this new formulation to approximate the problem by a separable ordinary differential equation whose closed-form solution captures the multiscale behaviour with sufficient accuracy and simplicity that it can be readily used to model the tip behaviour in hydraulic fracture simulators such as ILSA (Peirce & Detournay 2008). Applications of the proposed formulation are not limited to the class of multiscale semi-infinite hydraulic fracture problems described above but include other similar problems. To demonstrate this, § 3 considers the problem of a buoyancy-driven plane strain hydraulic fracture (see, e.g. Spence & Turcotte 1985, Lister 1990, Roper & Lister 2007) by rewriting the governing equations in terms of a single integral equation with a non-singular kernel.

## 2. A semi-infinite hydraulic fracture with leak-off

### 2.1. Problem formulation and regimes of propagation

We consider the problem of a one-dimensional semi-infinite hydraulic fracture propagating with a velocity  $V$  under plane strain elastic conditions (Garagash *et al.* 2011). To deal with this problem, it is convenient to introduce a moving coordinate system, in which the fracture tip is always located at the origin and the  $x$  denotes the distance from a point inside the fracture to the tip. As follows from Peirce & Detournay (2008) and Garagash *et al.* (2011), the lubrication equation that describes the fluid flow along the fracture can be written as

$$\frac{w^2}{\mu'} \frac{dp}{dx} = V + 2C'V^{1/2} \frac{x^{1/2}}{w}, \quad (2.1)$$

where  $w$  is the fracture width,  $p$  is the fluid pressure,  $V$  is the fracture propagation velocity, while  $\mu' = 12\mu$  is the scaled fluid viscosity and  $C' = 2C_L$  is the scaled Carter leak-off coefficient. We note a typographical error in Garagash *et al.* (2011), in which the factor of two is missing in front of the leak-off term in (2.1), which propagates into the remaining results. Assuming that the rock is a linear elastic medium, the equilibrium of the rock surrounding the fracture can be expressed as the following integral equation which relates the fluid pressure to the fracture width:

$$p(x) = \frac{E'}{4\pi} \int_0^\infty \frac{dw(s)}{ds} \frac{ds}{x-s}, \quad (2.2)$$

where  $E' = E/(1 - \nu^2)$  is the plane strain elastic modulus. The latter equation can be inverted (Garagash & Detournay 2000) to obtain

$$w = \frac{K'}{E'} x^{1/2} + \frac{4}{\pi E'} \int_0^\infty K(x, s) p(s) ds, \quad (2.3)$$

where  $K' = \sqrt{32/\pi} K_{Ic}$ ,  $K_{Ic}$  denotes the fracture toughness and the kernel is given by

$$K(x, s) = \ln \left| \frac{x^{1/2} + s^{1/2}}{x^{1/2} - s^{1/2}} \right| - 2 \frac{x^{1/2}}{s^{1/2}}. \quad (2.4)$$

To close the system (2.1) and (2.3), one needs to include a fracture propagation criterion, which states that

$$w = \frac{K'}{E'} x^{1/2}, \quad x \rightarrow 0. \quad (2.5)$$

As can be seen from (2.5), the fracture width vanishes at the fracture tip. This implies that the pressure gradient in (2.1) should be infinite at the tip to ensure that the fracture velocity is finite. This feature makes the system (2.1), (2.3) and (2.5) challenging to solve numerically.

An asymptotic analysis of (2.1), (2.3) and (2.5) shows that there are three limiting regimes of propagation, namely toughness (denoted by  $k$ ), leak-off (denoted by  $\tilde{m}$ ) and viscous (denoted by  $m$ ) (see, e.g. Garagash *et al.* 2011). The toughness regime corresponds to the situation in which the effects of fluid viscosity and leak-off can be neglected. The leak-off propagation regime occurs in situations when both the fracture

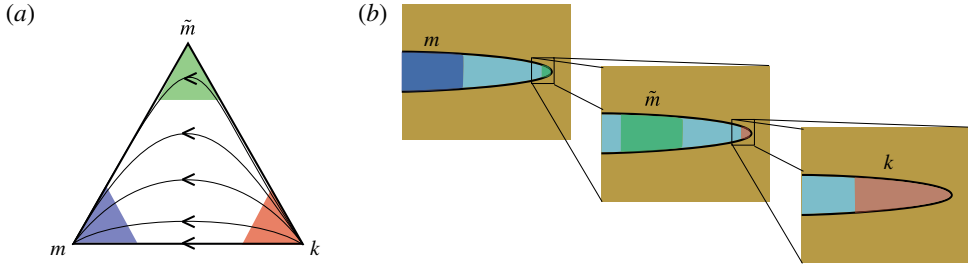


FIGURE 1. (a) The parametric triangle (after Garagash *et al.* 2011), which indicates three regimes of propagation: the toughness regime ( $k$  vertex), the leak-off regime ( $\tilde{m}$  vertex) and the viscous regime ( $m$  vertex). Lines inside the triangle show possible trajectories (assuming a spatial coordinate increasing away from the tip) in parametric space. (b) The schematics of a fracture and the regions where the asymptotic solutions apply.

toughness is small and the fluid flow inside the fracture is primarily balanced by the flux due to the fluid leaking into the surrounding rock. The viscous propagation regime corresponds to the situation in which both the fracture toughness and the leak-off are negligible. These asymptotic (vertex) solutions are respectively given by

$$w_k = \frac{K'}{E'} x^{1/2}, \quad w_{\tilde{m}} = \beta_{\tilde{m}} \left( \frac{4\mu^2 VC^2}{E'^2} \right)^{1/8} x^{5/8}, \quad w_m = \beta_m \left( \frac{\mu' V}{E'} \right)^{1/3} x^{2/3}, \quad (2.6a-c)$$

where  $\beta_{\tilde{m}} = 4/(15^{1/4}(\sqrt{2}-1)^{1/4})$  and  $\beta_m = 2^{1/3}3^{5/6}$ .

Knowledge of only the vertex solutions is not sufficient, since hydraulic fractures are known to transition from one vertex to another (Detournay 2004). With regard to the semi-infinite hydraulic fracture problem under consideration, these regimes occur at different length scales within the fracture, see figure 1. The toughness regime is present near the fracture tip, and, as one moves further from the tip (if the leak-off is significant), the leak-off regime appears, followed by the viscous regime at infinity. The transition is often schematically illustrated as a path inside a parametric triangle (Garagash *et al.* 2011), see figure 1. Vertices represent single-process limiting solutions (2.6), while lines with arrows indicate possible transition paths from the  $k$  vertex (near the tip) to the  $m$  vertex (far-field behaviour). It should be noted that without leak-off the transition occurs solely along the  $mk$  edge, while in the case of large leak-off the transition occurs along the  $\tilde{m}k$  and  $m\tilde{m}$  edges. The coloured zones inside the triangle indicate the regions of applicability of the vertex solutions. To determine the solution in the transition regimes (the inner white area of the parametric triangle), one has to solve (2.1), (2.3) and (2.5) numerically. The numerical analysis of this problem has proven to be very challenging due to the multiple length scales involved and the singular behaviour of the fluid pressure at the tip. This study introduces an alternative approach, which allows us to avoid solving a singular problem and enables us to find the fracture geometry at all length scales in a numerically efficient way.

## 2.2. Alternative problem formulation and numerical solution

One of the biggest obstacles to solving the system of (2.1), (2.3) and (2.5) numerically lies in an accurate evaluation of the flux in (2.1), given that the fluid pressure is

*A non-singular integral equation formulation*

singular at the fracture tip. To mitigate the problem, this section aims to rewrite the system of equations in a form in which the fluid pressure does not enter the problem. We first note that the elasticity equation (2.3) can be integrated by parts to yield

$$w = \frac{K'}{E'}x^{1/2} - \frac{4}{\pi E'} \int_0^\infty F(x, s) \frac{dp}{ds} ds, \quad (2.7)$$

where

$$K(x, s) = \frac{\partial F(x, s)}{\partial s}, \quad F(x, s) = (s - x) \ln \left| \frac{x^{1/2} + s^{1/2}}{x^{1/2} - s^{1/2}} \right| - 2x^{1/2}s^{1/2}. \quad (2.8a,b)$$

It should be noted here that

$$\lim_{s \rightarrow \infty} F(x, s)p(s) = 4x \lim_{s \rightarrow \infty} p(s) = 0, \quad \lim_{s \rightarrow 0} F(x, s)p(s) = -4x^{1/2} \lim_{s \rightarrow 0} s^{1/2}p(s) = 0, \quad (2.9a,b)$$

since for the viscous far-field solution  $p(s) \propto s^{-1/3}$  as  $s \rightarrow \infty$  and for the toughness near-tip solution  $p(s) \propto \ln(s)$  as  $s \rightarrow 0$ , see, e.g. Garagash *et al.* (2011). Then, the pressure gradient can be substituted into (2.7) from the lubrication equation (2.1) to find

$$w(x) = \frac{K'}{E'}x^{1/2} - \frac{4}{\pi E'} \int_0^\infty F(x, s) \frac{\mu'}{w(s)^2} \left[ V + 2C'V^{1/2} \frac{s^{1/2}}{w(s)} \right] ds. \quad (2.10)$$

Equation (2.10) is an integral equation for  $w(x)$  only, which already simplifies the original problem since the pressure, which is singular at the tip, is not a part of the solution. It should be noted that a similar integration by parts was also performed in Spence, Sharp & Turcotte (1987) and Lister (1990). Moreover, an equation similar to (2.10) was formulated in Spence *et al.* (1987), but it was only used for the asymptotic analysis. By introducing the scaled quantities

$$\tilde{w} = \frac{E'w}{K'x^{1/2}}, \quad \chi = \frac{2C'E'}{V^{1/2}K'}, \quad \tilde{x} = (x/l)^{1/2}, \quad \tilde{s} = (s/l)^{1/2}, \quad l = \left( \frac{K'^3}{\mu'E'^2V} \right)^2, \quad (2.11a-e)$$

equation (2.10) can be further reduced to

$$\tilde{w}(\tilde{x}) = 1 + \frac{8}{\pi} \int_0^\infty G(\tilde{s}/\tilde{x}) \left[ \frac{1}{\tilde{w}(\tilde{s})^2} + \frac{\chi}{\tilde{w}(\tilde{s})^3} \right] d\tilde{s}, \quad (2.12)$$

where  $l$  is the length scale, the dimensionless parameter  $\chi$  characterizes the leak-off and the kernel is

$$G(t) = \frac{1-t^2}{t} \ln \left| \frac{1+t}{1-t} \right| + 2. \quad (2.13)$$

It should be noted that a similar length scale  $l$  is used in Garagash *et al.* (2011) to describe the transition regime along the  $mk$  edge (denoted by  $l_{mk}$  there). In this scaling, the propagation condition (2.5) reduces to

$$\tilde{w}(0) = 1. \quad (2.14)$$

Given the fact that the kernel  $G(t)$  is positive and not singular ( $G(0) = 4$ ,  $G(t) \approx 4/(3t^2)$  for  $t \gg 1$ ), and that  $\tilde{w} \geq 1$ , the integral equation (2.12) is amenable to direct numerical solution, without introducing any asymptotic behaviour into the solution.

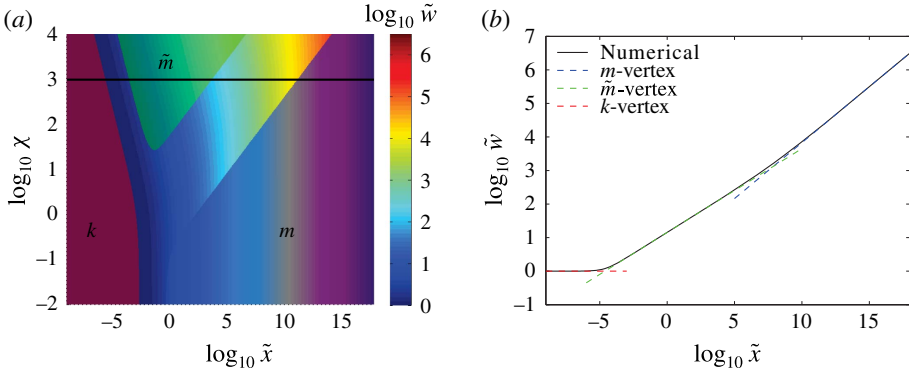


FIGURE 2. (a) Variation of the scaled fracture opening  $\tilde{w}$  versus the scaled distance  $\tilde{x}$  and leak-off parameter  $\chi$ . The red, green and blue areas indicate the regions of applicability of the toughness, leak-off and viscous vertex solutions (2.15). The black line indicates the solution that corresponds to  $\chi = 10^3$ . (b) Numerical solution for  $\chi = 10^3$  versus  $\tilde{x}$  (black line) and vertex asymptotic solutions  $m$  (viscous, blue line),  $\tilde{m}$  (leak-off, green line) and  $k$  (toughness, red line).

It is instructive to check whether the vertex solutions can be deduced directly from (2.12). The first term on the right-hand side of (2.12) represents the effect of fracture toughness, the second term (the first term under the integral sign) represents the effect of the fluid viscosity and the third term represents the effect of leak-off. By substituting  $\tilde{w} = C\tilde{x}^\alpha$  into (2.12) and keeping only one term that corresponds to either toughness, viscosity or leak-off, we obtain

$$\tilde{w}_k = 1, \quad \tilde{w}_{\tilde{m}} = \beta_{\tilde{m}}\chi^{1/4}\tilde{x}^{1/4}, \quad \tilde{w}_m = \beta_m\tilde{x}^{1/3}, \quad (2.15a-c)$$

which correspond exactly to the asymptotic solutions (2.15) in the scaled coordinates. It should be noted here that the values of  $\beta_m$  and  $\beta_{\tilde{m}}$  are calculated based on the fact that

$$\int_0^\infty \frac{G(t)}{t^\alpha} dt = \frac{2\pi}{\alpha(2-\alpha)} \tan\left(\frac{\pi}{2}\alpha\right), \quad (2.16)$$

where  $-1 < \alpha < 1$  (the integral does not converge for values of  $\alpha$  that are outside this interval).

In order to solve (2.12) numerically, the integral is discretized using Simpson’s rule, and the resultant system of nonlinear algebraic equations is solved using Newton’s method. To capture all the length scales present in the solution, grid points are distributed uniformly on a logarithmic scale. To mitigate the error caused by a finite upper limit of the integral in (2.12), the fracture opening solution that corresponds to the last several grid points (on the logarithmic scale) is discarded. Figure 2(a) shows the variation of the solution,  $\tilde{w}$ , versus  $\chi$  and  $\tilde{x}$ . To indicate the regions of applicability of the vertex solutions (2.15), these solutions are shifted upwards by  $10^{-2}$  on a log scale (to highlight regions where the relative difference between the numerical and asymptotic solutions is smaller than 2.3%) and then superimposed on the numerical solution. It should be noted that this map of the regimes is very similar to the schematics in Garagash *et al.* (2011). Figure 2(b) shows the variation of the scaled fracture opening versus  $\tilde{x}$  for  $\chi = 10^3$ , which corresponds to the black line shown in figure 2(a). The vertex asymptotic solutions are superimposed. One can

### *A non-singular integral equation formulation*

observe a transition from the toughness-dominated regime, to the leak-off and, finally, to the viscous-dominated regime. This transition is consistent with the schematics shown in figure 1.

#### *2.3. Approximate analytical solution*

Numerical solution of (2.12) provides an accurate way of solving the problem under consideration. For some practical applications, e.g. for implementing this solution in a hydraulic fracturing simulator such as ILSA (Peirce & Detournay 2008), it is desirable to obtain an easily evaluated approximate solution that is reasonably accurate. To derive such an approximate solution, one can differentiate (2.12) to obtain

$$\frac{d\tilde{w}(\tilde{x})}{d\tilde{x}} = -\frac{8}{\pi} \int_0^\infty G'(\tilde{s}/\tilde{x}) \frac{\tilde{s}}{\tilde{x}^2} \left[ \frac{1}{\tilde{w}(\tilde{s})^2} + \frac{\chi}{\tilde{w}(\tilde{s})^3} \right] d\tilde{s}, \quad \tilde{w}(0) = 1. \quad (2.17)$$

Knowing that the solution has a form  $\tilde{w} \propto \tilde{x}^\delta$ , where  $0 \leq \delta \leq 1/3$  varies slowly with  $\tilde{x}$ , one can rewrite the latter equation as

$$\frac{d\tilde{w}(\tilde{x})}{d\tilde{x}} = -\frac{8}{\pi} \int_0^\infty G'(\tilde{s}/\tilde{x}) \frac{\tilde{x}^{2\delta-1}}{\tilde{s}^{2\delta-1}} \frac{d\tilde{s}}{\tilde{x}} \left[ \frac{\tilde{s}^{2\delta}}{\tilde{w}(\tilde{s})^2 \tilde{x}^{2\delta}} \right] - \frac{8}{\pi} \int_0^\infty G'(\tilde{s}/\tilde{x}) \frac{\tilde{x}^{3\delta-1}}{\tilde{s}^{3\delta-1}} \frac{d\tilde{s}}{\tilde{x}} \left[ \frac{\chi \tilde{s}^{3\delta}}{\tilde{w}(\tilde{s})^3 \tilde{x}^{3\delta}} \right]. \quad (2.18)$$

The terms in square brackets vary slowly with  $\tilde{s}$ . Moreover, the function  $G'(t)/t^\alpha$  ( $t = \tilde{s}/\tilde{x}$ ,  $\alpha$  is some power) resembles a Delta function on a logarithmic scale. For these reasons, one can approximate (2.18) by replacing the integral kernels by the appropriate Delta functions, and arrive at the following implicit first-order ordinary differential equation:

$$\tilde{w}' = \frac{C_1(\delta)}{\tilde{w}^2} + \frac{\chi C_2(\delta)}{\tilde{w}^3}, \quad \delta = \tilde{x} \frac{\tilde{w}'}{\tilde{w}}, \quad \tilde{w}(0) = 1, \quad (2.19a-c)$$

where the coefficients  $C_1$  and  $C_2$  are calculated using (2.16) as

$$C_1(\delta) = \frac{4(1-2\delta)}{\delta(1-\delta)} \tan(\pi\delta), \quad C_2(\delta) = \frac{16(1-3\delta)}{3\delta(2-3\delta)} \tan\left(\frac{3\pi}{2}\delta\right). \quad (2.20a,b)$$

The coefficients  $C_1$  and  $C_2$  vary monotonically and slowly with  $\delta$  (note that  $0 \leq \delta \leq 1/3$ ). For instance,  $C_1(0) = C_2(0) = 4\pi \approx 12.6$ ,  $C_1(1/3) = \beta_m^3/3 \approx 10.4$ , while  $C_2(1/3) = 32/\pi \approx 10.2$ . Due to the small variations in the magnitudes of  $C_1$  and  $C_2$ , one may treat them as constants, in which case (2.19) reduces to a separable differential equation, whose implicit solution is

$$\tilde{w}^3 - 1 - \frac{3}{2}b(\tilde{w}^2 - 1) + 3b^2(\tilde{w} - 1) - 3b^3 \ln\left(\frac{b + \tilde{w}}{b + 1}\right) = 3C_1(\delta)\tilde{x}, \quad b = \frac{C_2(\delta)}{C_1(\delta)}\chi. \quad (2.21)$$

To obtain a zeroth-order approximate solution from (2.21), one may use a constant approximation for  $\delta$ . Since the  $1/\tilde{w}^2$  term in (2.19) is important for the viscous solution, for which  $\delta = 1/3$ , one may take  $C_1(1/3) = \beta_m^3/3$ . Since the  $\chi/\tilde{w}^3$  term is important for the leak-off regime, for which  $\delta = 1/4$ , one may take  $C_2(1/4) = \beta_m^4/4$ . In this case, the zeroth-order solution,  $\tilde{w}_0$ , can be obtained from

$$\tilde{w}_0^3 - 1 - \frac{3}{2}b_0(\tilde{w}_0^2 - 1) + 3b_0^2(\tilde{w}_0 - 1) - 3b_0^3 \ln\left(\frac{b_0 + \tilde{w}_0}{b_0 + 1}\right) = \beta_m^3\tilde{x}, \quad b_0 = \frac{3\beta_m^4}{4\beta_m^3}\chi \approx 0.9912\chi. \quad (2.22)$$

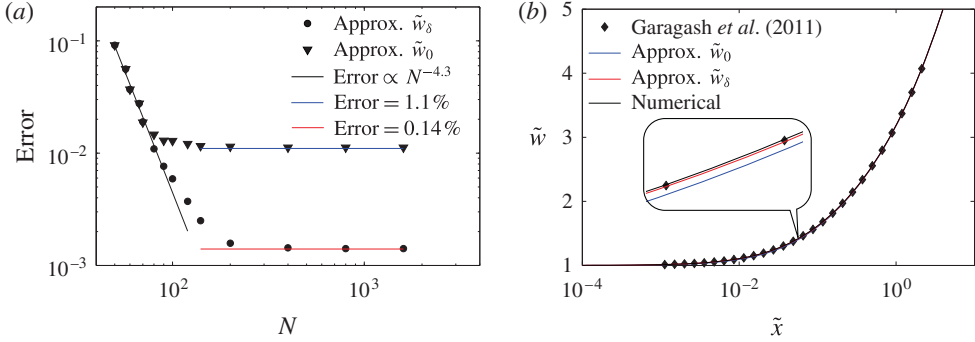


FIGURE 3. (a) The discrepancy of the zeroth-order solution  $\tilde{w}_0$  and the  $\delta$ -correction  $\tilde{w}_\delta$  compared with the numerical solution versus the number of elements used in the numerical solution  $N$ . (b) Variation of the scaled fracture width versus  $\tilde{x}$  for  $\chi = 0$  ( $mk$  edge): calculated by Garagash *et al.* (2011) (markers), zeroth-order approximation (blue line),  $\delta$ -correction (red line) and the numerical solution (black line).

It can be easily shown that the zeroth-order solution captures all vertex solutions (2.15) precisely and describes the transition regions approximately. To obtain a correction that accounts for different values of  $\delta$ , a so-called  $\delta$ -correction, one may use (2.19) (with  $C_1(1/3) = \beta_m^3/3$  and  $C_2(1/4) = \beta_m^4/4$ ) to calculate  $\delta$  as

$$\delta = \frac{\beta_m^3 \tilde{x}(\tilde{w}_0)}{3\tilde{w}_0^3} \left( 1 + \frac{b_0}{\tilde{w}_0} \right), \quad (2.23)$$

where  $\tilde{x}(\tilde{w}_0)$  is calculated using (2.22). By substituting (2.23) into (2.21), one may obtain a  $\delta$ -corrected solution  $\tilde{w}_\delta$ . It is possible to continue the iteration procedure, but one iteration is sufficient for all practical applications.

It is also possible to obtain simple expressions for two out of the three edge solutions, see the parametric triangle in figure 1. To find the approximate solution that corresponds to the  $mk$  edge (no leak-off), let  $\chi = 0$ , then (2.21) and (2.23) can be simplified to

$$\tilde{w}_{\delta,mk} = (1 + 3C_1(\delta)\tilde{x})^{1/3}, \quad \delta = \frac{1}{3} \frac{\beta_m^3 \tilde{x}}{1 + \beta_m^3 \tilde{x}}, \quad (2.24a,b)$$

while the zeroth-order solution is simply  $\tilde{w}_{0,mk} = (1 + \beta_m^3 \tilde{x})^{1/3}$ . To find the approximation for the  $\tilde{m}k$  solution, one can take  $\chi \gg 1$  to simplify (2.21) and (2.23) as

$$\tilde{w}_{\delta,\tilde{m}k} = (1 + 4\chi C_2(\delta)\tilde{x})^{1/4}, \quad \delta = \frac{1}{4} \frac{\beta_m^4 \chi \tilde{x}}{1 + \beta_m^4 \chi \tilde{x}}. \quad (2.25a,b)$$

The corresponding zeroth-order solution is  $\tilde{w}_{0,\tilde{m}k} = (1 + \chi \beta_m^4 \tilde{x})^{1/4}$ . Unfortunately, it is not possible to extract a simple explicit solution for the  $\tilde{m}\tilde{m}$  edge from (2.21).

To illustrate the accuracy of the approximate analytical solution, figure 3(a) shows the errors of the zeroth-order approximate solution and the  $\delta$ -corrected solution, defined respectively as  $\max\{|\tilde{w}_\delta - \tilde{w}|/\tilde{w}\}$  and  $\max\{|\tilde{w}_0 - \tilde{w}|/\tilde{w}\}$ , where  $\tilde{w}$  is the numerical solution that is calculated using  $N$  points in  $\tilde{x}$ . Here, the maximum is

calculated over  $10^{-8} \leq \tilde{x} \leq 10^{18}$  and  $10^{-2} \leq \chi \leq 10^4$ , which corresponds to the parameter span shown in figure 2. For small values of  $N$ , the error due to numerical discretization dominates, and one can observe a convergence rate of approximately 4, which reflects the fact that Simpson’s rule is used to discretize the integral in (2.12). For larger values of  $N$ , the discretization error becomes smaller than the errors corresponding to the approximate solutions. This leads to an error ‘saturation’, at which the limiting values of the error reflect the accuracy of the approximate solution. The zeroth-order solution,  $\tilde{w}_0$ , has an accuracy of approximately 1.1%, while the  $\delta$ -correction,  $\tilde{w}_\delta$ , substantially increases the accuracy to 0.14%. Since the approximate solutions are able to capture all vertex solutions precisely, the error is concentrated in the transition zones. For both approximations, the maximum error is reached in the transition from the  $k$  to the  $m$  vertex, which corresponds to  $\chi = 0$  and  $\tilde{x} \approx 10^{-1.5}$ . Figure 3(b) shows the variation of the scaled fracture opening versus  $\tilde{x}$  for  $\chi = 0$ , i.e. along the  $mk$  edge. A comparison is made between the numerical solution by Garagash *et al.* (2011), the numerical solution of (2.12), as well as two approximations  $\tilde{w}_0$  and  $\tilde{w}_\delta$  stemming from (2.24). All solutions agree well with one another, although  $\tilde{w}_0$  is clearly less accurate than  $\tilde{w}_\delta$ .

### 3. Buoyancy-driven plane strain fracture

To illustrate the versatility of the approach developed in §2.2, this section aims to analyse the problem of a buoyancy-driven hydraulic fracture (Spence *et al.* 1987; Roper & Lister 2007). As follows from Roper & Lister (2007), the lubrication equation (2.1), in this case, needs to be replaced by

$$\frac{w^2}{\mu'} \left( \frac{dp}{dx} + \Delta\rho g \right) = V, \quad (3.1)$$

where the leak-off is removed and the  $\Delta\rho g$  term captures the effect of buoyancy. Here,  $\Delta\rho$  is the difference between the mass densities of the rock and the fracturing fluid, while  $g$  denotes the gravitational acceleration. By using a similar procedure to that in §2.2 (including notation and scaling (2.11)), the analogue of (2.12) becomes

$$\tilde{w}(\tilde{x}) = 1 + \frac{8}{\pi} \int_0^\infty G(\tilde{s}/\tilde{x}) \left[ \frac{1}{\tilde{w}(\tilde{s})^2} - \tilde{g}\tilde{s}^2 \right] d\tilde{s}, \quad \tilde{g} = \frac{\Delta\rho g l^{3/2}}{K'}, \quad (3.2)$$

where  $\tilde{g}$  is the normalized gravity and  $l$  is the length scale defined in (2.11). The integral equation (3.2) is solved numerically by using Simpson’s rule to discretize the integral and Newton’s method to solve the system of nonlinear algebraic equations. Since the integral  $\int_0^\infty G(\tilde{s}/\tilde{x})\tilde{s}^2 d\tilde{s}$  does not converge, it is essential to keep both terms under the integral sign in (3.2) together. It should also be noted that an ordinary differential equation similar to (2.19) can be derived from (3.2). Its solution is less accurate (since the assumption  $\tilde{w} \propto \tilde{x}^\delta$  is no longer valid), but is used as an initial guess for Newton’s method.

In order to compare the results with the numerical solution (Peirce 2010), which uses a Hermite cubic collocation scheme, we first make a conversion between scaled variables. The normalized fracture toughness,  $K$ , the normalized fracture half-width,  $H$ , and the normalized coordinate,  $X$ , used in Peirce (2010) are related to our variables as

$$K = \frac{1}{2}\tilde{g}^{1/8}, \quad H = 2^{4/3}\tilde{g}^{1/3}\tilde{x}\tilde{w}, \quad X = 2^{5/3}\tilde{g}^{2/3}\tilde{x}^2. \quad (3.3a-c)$$

It should be noted that Roper & Lister (2007) give the asymptotic solution  $H_0 = (X^{1/2}(2 - X)^{3/2})/2$  (valid for  $K \gg 1$ ) in terms of the aforementioned quantities (3.3).

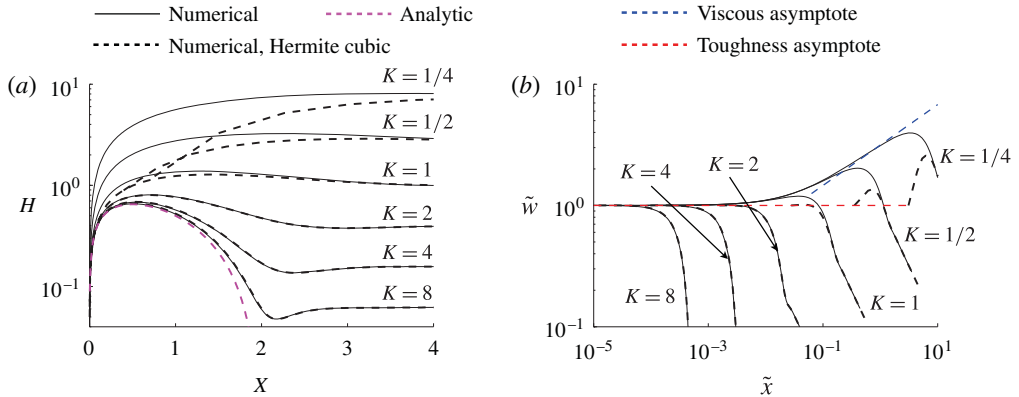


FIGURE 4. Comparison between the numerical solution of (3.2) (black solid lines) and the numerical solution by Peirce (2010) (black dashed lines) for the buoyancy-driven hydraulic fracture for different values of  $K$ . (a) Solutions written in terms of the scaling in Peirce (2010), see (3.3); the magenta dashed line indicates the approximate solution  $H_0 = (X^{1/2}(2 - X)^{3/2})/2$  (valid for  $K \gg 1$ ) (Roper & Lister 2007). (b) Solutions written in terms of the scaling (2.11); the blue and red dashed lines indicate the viscous and toughness asymptotic solutions (2.15) respectively. The solution by Peirce (2010) works poorly for small  $K$ .

Figure 4(a) compares the numerical solution of (3.2) (black solid lines) with the numerical solution by Peirce (2010) (black dashed lines) for different values of the normalized fracture toughness  $K$ . The analytic solution  $H_0$  is represented by the dashed magenta line. Figure 4(b) compares the same solutions, but in terms of the quantities  $\tilde{w}$  and  $\tilde{x}$ , and plotted on a log–log scale. The viscous and toughness asymptotic solutions (2.15) are represented by dashed blue and red lines respectively. Both numerical algorithms give nearly identical results for large values of the normalized fracture toughness  $K$ . At the same time, there is a visible difference for  $K \leq 1$ . This happens because the algorithm in Peirce (2010) is designed to capture the toughness propagation regime and relies on the toughness asymptotic solution for the tip element; see figure 4(b), where all dashed black lines originate from the toughness asymptote (shown by the dashed red line). The toughness asymptotic solution works poorly in situations when the transition from the toughness to the viscous regime of propagation happens on a length scale comparable to the element size, as indicated in figure 4. At the same time, the new numerical formulation works well for all values of  $K$ .

#### 4. Summary

This paper introduces an alternative formulation for the multiscale analysis of a steadily propagating semi-infinite hydraulic fracture. The key feature of the approach lies in rewriting the system of governing equations as a single integral equation with a non-singular kernel, whose solution is directly related to the fracture width. This approach is used to provide an accurate numerical solution for a propagating semi-infinite hydraulic fracture with leak-off. Because the new formulation features a non-singular kernel, and does not involve a calculation of the fluid pressure, standard numerical techniques are used to obtain accurate results rapidly. The resulting numerical solution is able to resolve multiscale behaviour and to capture all known

asymptotic solutions of the problem. This approach is also used to reduce the problem to an approximate separable ordinary differential equation whose analytic solution captures all known asymptotic solutions of the problem exactly, and provides a highly accurate estimation of the fracture width in transition regions. To highlight the versatility of the new formulation, it is applied to solve the problem of a steadily propagating semi-infinite buoyancy-driven plane strain hydraulic fracture. The results agree well with published numerical solutions that were developed for the toughness-dominated regime of propagation. In addition, the multiscale behaviour at the fracture tip, associated with the transition from the toughness to the viscous regime of propagation, is easily captured using the new formulation.

## Acknowledgements

The support of the British Columbia Oil and Gas Commission and the NSERC discovery grants programme is gratefully acknowledged.

## References

- CARTER, E. D. 1957 Optimum fluid characteristics for fracture extension. In *Drilling and Production Practices* (ed. G. C. Howard & C. R. Fast), pp. 261–270. American Petroleum Institute.
- DESROCHES, J., DETOURNAY, E., LENOACH, B., PAPANASTASIOU, P., PEARSON, J. R. A., THIERCELIN, M. & CHENG, A. H.-D. 1994 The crack tip region in hydraulic fracturing. *Proc. R. Soc. Lond. A* **447**, 39–48.
- DETOURNAY, E. 2004 Propagation regimes of fluid-driven fractures in impermeable rocks. *Intl J. Geomech.* **4**, 35–45.
- GARAGASH, D. & DETOURNAY, E. 2000 The tip region of a fluid-driven fracture in an elastic medium. *J. Appl. Mech.* **67**, 183–192.
- GARAGASH, D. I., DETOURNAY, E. & ADACHI, J. I. 2011 Multiscale tip asymptotics in hydraulic fracture with leak-off. *J. Fluid Mech.* **669**, 260–297.
- GORDELIY, E. & PEIRCE, A. P. 2013 Implicit level set schemes for modeling hydraulic fractures using the XFEM. *Comput. Meth. Appl. Mech. Engng* **266**, 125–143.
- KOVALYSHEN, Y. & DETOURNAY 2013 Propagation of a semi-infinite hydraulic fracture in a poroelastic medium. In *Poromechanics V – Proceedings of the 5th Biot Conference on Poromechanics*, pp. 431–437.
- LECAMPION, B., PEIRCE, A. P., DETOURNAY, E., ZHANG, X., CHEN, Z., BUNGER, A. P., DETOURNAY, C., NAPIER, J., ABBAS, S., GARAGASH, D. & CUNDALL, P. 2013 The impact of the near-tip logic on the accuracy and convergence rate of hydraulic fracture simulators compared to reference solutions. In *Effective and Sustainable Hydraulic Fracturing* (ed. A. P. Bunger, J. McLennan & R. Jeffrey), chap. 43, pp. 855–873. Intech, ISBN: 978-953-51-1137-5.
- LENOACH, B. 1995 The crack tip solution for hydraulic fracturing in a permeable solid. *J. Mech. Phys. Solids* **43**, 1025–1043.
- LISTER, J. R. 1990 Buoyancy-driven fluid fracture: the effects of material toughness and of low-viscosity precursors. *J. Fluid Mech.* **210**, 263–280.
- PEIRCE, A. 2010 A Hermite cubic collocation scheme for plane strain hydraulic fractures. *Comput. Meth. Appl. Mech. Engng* **199**, 1949–1962.
- PEIRCE, A. & DETOURNAY, E. 2008 An implicit level set method for modeling hydraulically driven fractures. *Comput. Meth. Appl. Mech. Engng* **197**, 2858–2885.
- PEIRCE, A. P. 2015 Modeling multi-scale processes in hydraulic fracture propagation using the implicit level set algorithm. *Comput. Meth. Appl. Mech. Engng* **283**, 881–908.
- ROPER, S. M. & LISTER, J. R. 2007 Buoyancy-driven crack propagation: the limit of large fracture toughness. *J. Fluid Mech.* **580**, 359–380.
- SPENCE, D., SHARP, P. & TURCOTTE, D. 1987 Buoyancy-driven crack propagation: a mechanism for magma migration. *J. Fluid Mech.* **174**, 135–153.
- SPENCE, D. & TURCOTTE, D. 1985 Magma-driven propagation of cracks. *J. Geophys. Res.* **90**, 575–580.